Geophysical Research Letters

Supporting Information for

The role of the North Atlantic Oscillation for projections of winter mean precipitation in Europe

C. M. McKenna[1] and A. C. Maycock [1]
[1] School of Earth and Environment, University of Leeds, Leeds, UK
Corresponding author: Christine McKenna (C.McKenna1@leeds.ac.uk)

Contents of this file

Introduction

This document contains tables and additional figures that provide further details on the datasets and methods used, the model evaluation process, and the results presented in the main text.

In particular, Table S1 provides details of the MMLEA model simulations used in the study. Table S2 provides details of the CMIP5 model simulations used in Figure S1. Figure S1 compares the intermodel spread in projections of future European mean winter precipitation change for the MMLEA models and the CMIP5 models. Figure S2 shows the historical winter NAO-MSLP and NAO-precipitation patterns for the MMLEA models and the observations; the modeled patterns are used in Figure 1 and Figure 4 to decompose MSLP and precipitation anomaly maps into an NAO-congruent part and a residual. Figure S3 evaluates the modeled NAO-precipitation relationships against the observations for area-average precipitation in northern and southern Europe. Figure S4 evaluates the modeled distributions of historical annual winter NAO index anomalies against the observed distribution. Figure S5 shows the maps from Figure 1b for all MMLEA models. Figure S6 explains the calculation of Figure 1c in further detail. Figure S7 shows a version of Figure 1 where the precipitation and MSLP changes are normalized by the change in global-mean surface air temperature. Figure S8 shows projected changes in the distributions of annual winter NAO index for selected MMLEA models. Figure S9 shows the maps from Figure 3b for all selected MMLEA models.

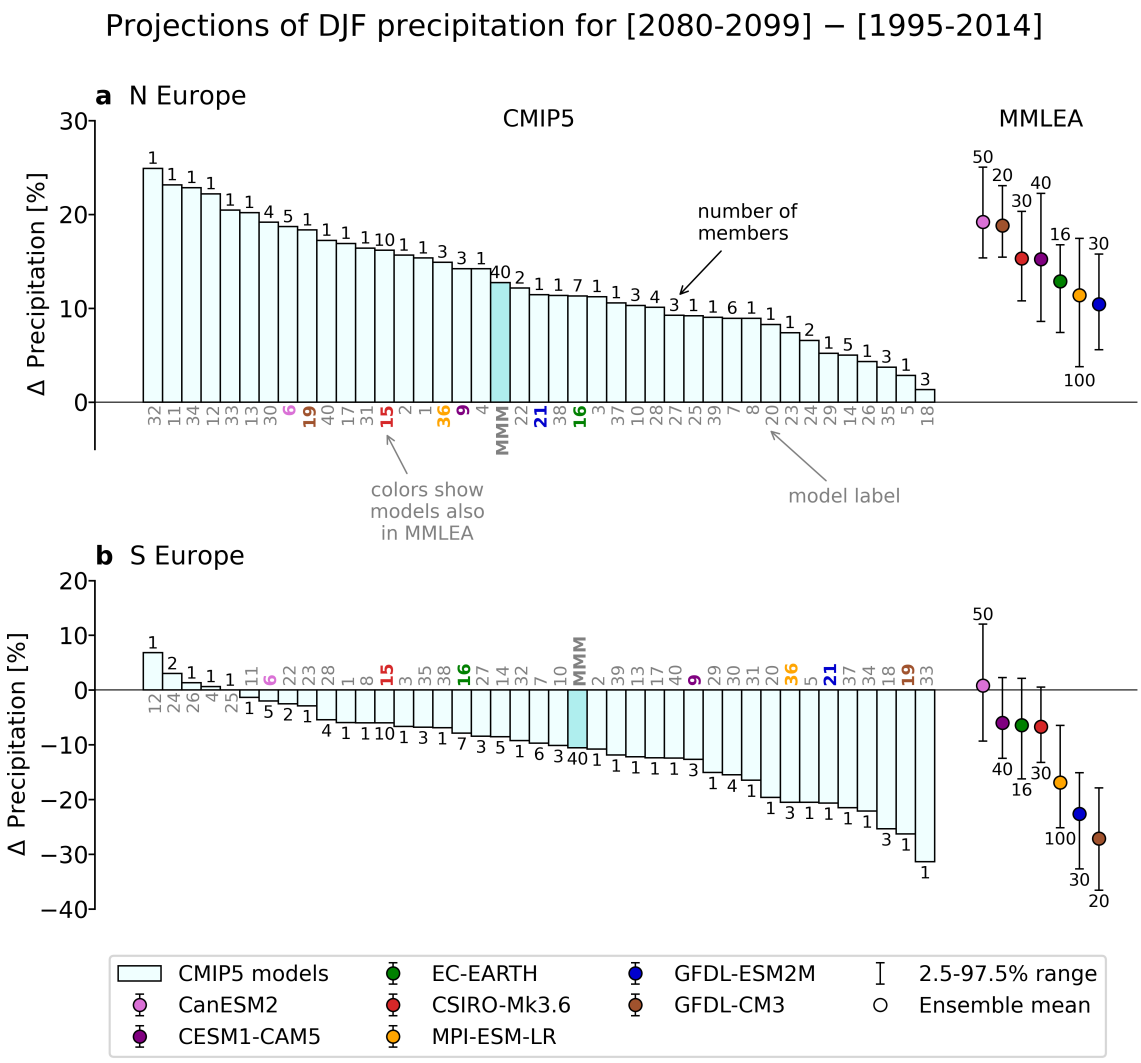

Figure S1: Projected change (2080-2099 minus 1995-2014) in mean winter precipitation in (a) northern Europe and (b) southern Europe, for the CMIP5 and MMLEA models under the RCP8.5 scenario. Precipitation anomalies are shown as a percentage of the 1995-2014 climatology. For CMIP5 models, ensemble means are shown if more than one ensemble member is available. Darker bar indicates the CMIP5 multimodel mean (MMM). Circles for MMLEA indicate the ensemble mean and whiskers indicate the 2.5%-97.5% range of responses across the ensemble members. A list of the CMIP5 model simulations used in this figure is given in Table S2.

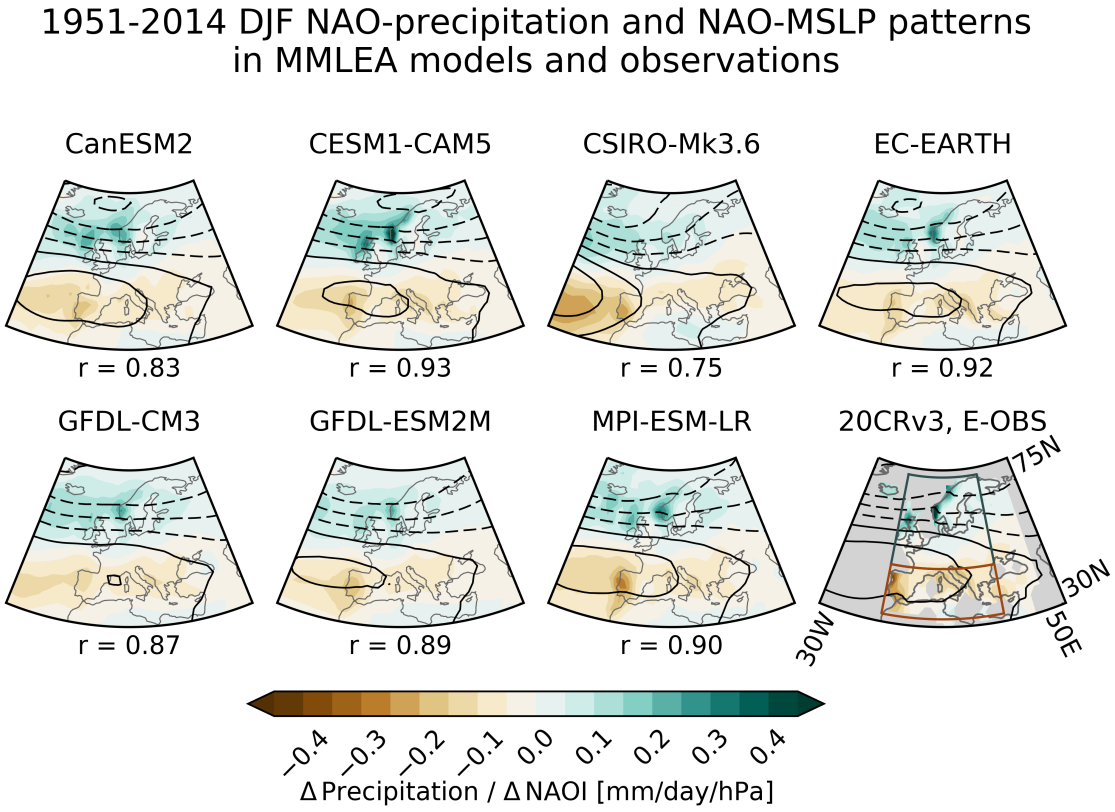

Figure S2: Historical (1951-2014) DJF NAO-precipitation (shading) and NAO-MSLP (contours) patterns in the MMLEA models and observations. Patterns are shown for a 1 hPa positive change in NAO index. MSLP contours range from −1.4 hPa (dashed) to 1 hPa (solid) in 0.4 hPa intervals. *r* is the area-weighted pattern correlation between the modeled and observed (20CRv3/E-OBS) NAO-precipitation patterns in regions where the observed pattern is not masked (non-gray shading). When calculating the observed NAO-precipitation pattern, masks are applied to any winter where more than one-third (30 days) of the E-OBS data is missing and any grid-cell where more than one-third (21 years) of winters are masked. Blue and brown boxes in the lower far-right panel define the northern and southern European regions used in the study, respectively.

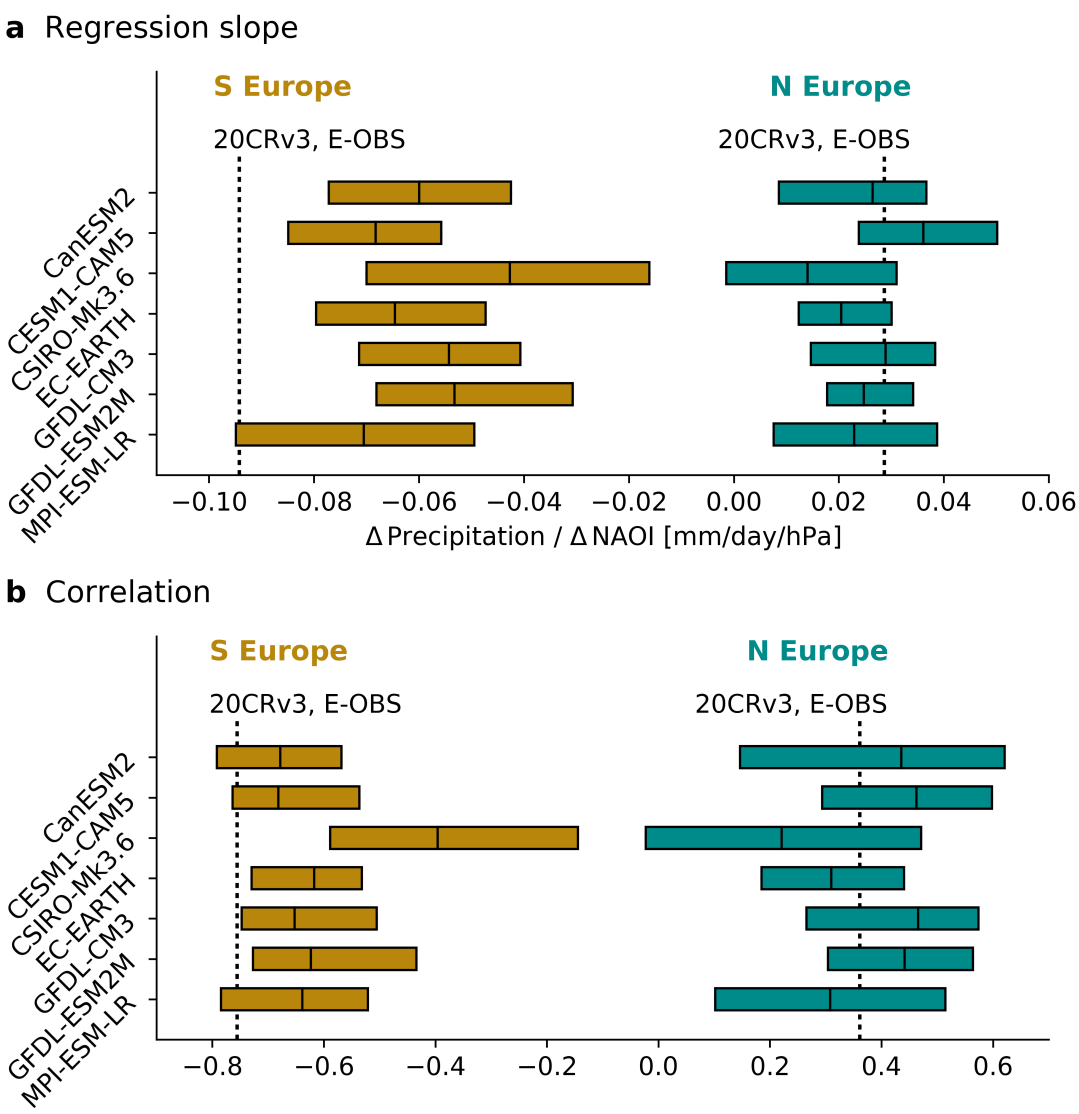

Figure S3: Historical (1951-2014) DJF NAO-precipitation relationships for area-average precipitation in northern (blue) and southern (brown) Europe: an evaluation of the MMLEA models against the observations. The relationships are evaluated in terms of (a) the regression slope (the parameter shown in Figure S2), and (b) the correlation coefficient. Colored boxes show the 2.5%-97.5% range and median value of each parameter across the ensemble members for each MMLEA model. Black vertical dashed lines show the values of each parameter for 20CRv3/E-OBS. Blue and brown boxes in the lower far-right panel of Figure S2 define the northern and southern European regions, respectively. Prior to calculating area-average northern and southern European precipitation for this figure, modeled data are masked in grid-cells where E-OBS data are masked (see Figure S2).

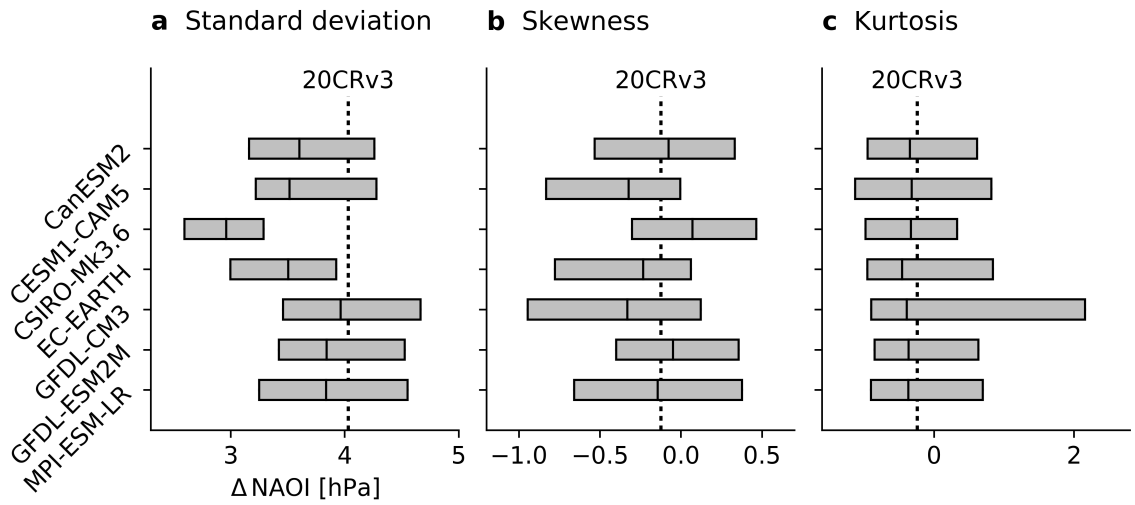

Figure S4: Summary statistics for the distribution of historical (1951-2014) annual DJF NAO index anomaly: an evaluation of the MMLEA models against the observations. The summary statistics evaluated are the (a) standard deviation, (b) skewness, and (c) kurtosis. Gray boxes show the 2.5%-97.5% range and median value of each statistic across the ensemble members for each MMLEA model. Black vertical dashed lines show the value of each statistic for 20CRv3. NAO index anomalies are defined relative to the 1995-2014 climatology.

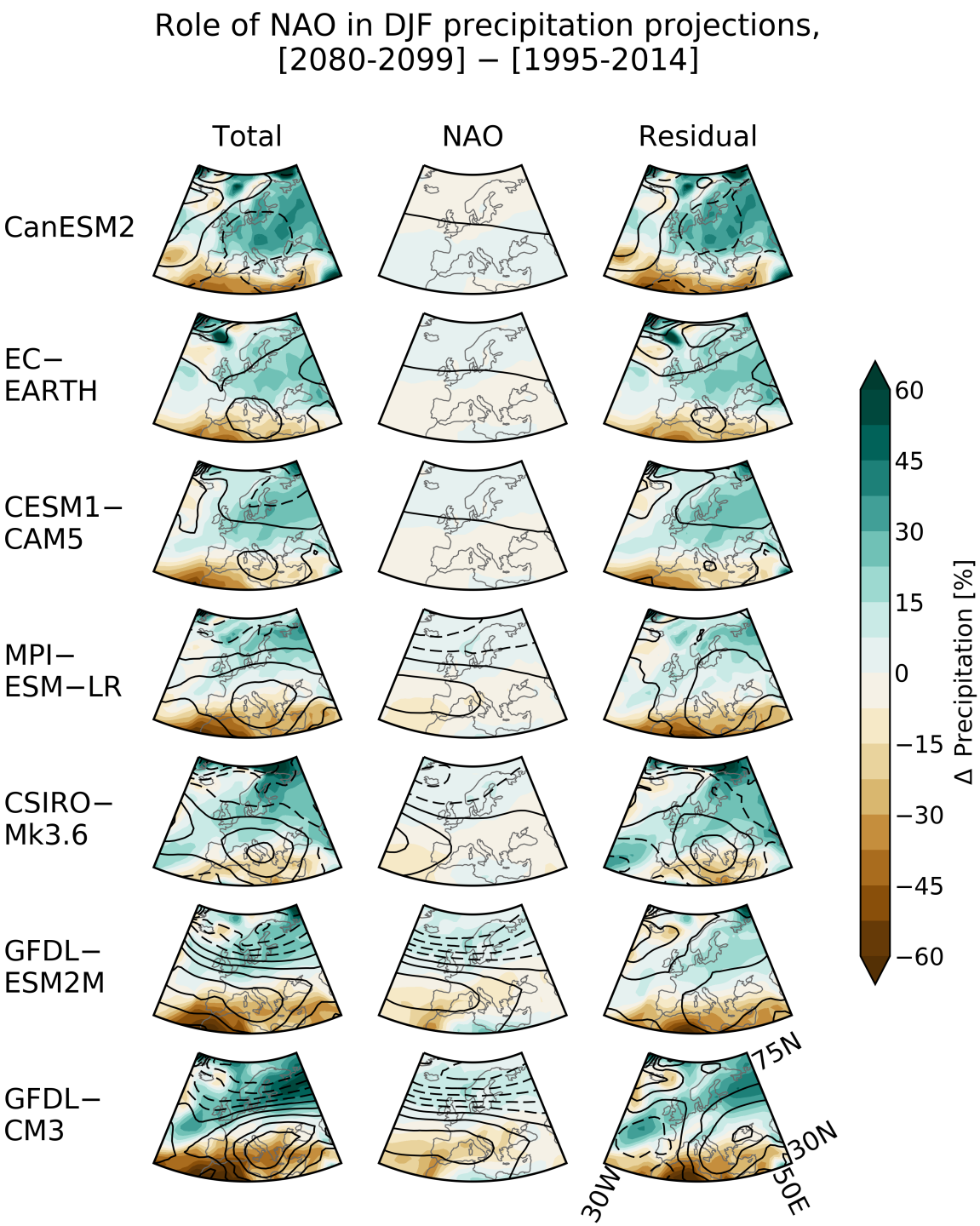

Figure S5: Maps in Figure 1b for all MMLEA models. Models are ordered from top to bottom with increasing forced DJF NAO index change. Contours range from −6 hPa (dashed) to 4 hPa (solid) in 1 hPa intervals.

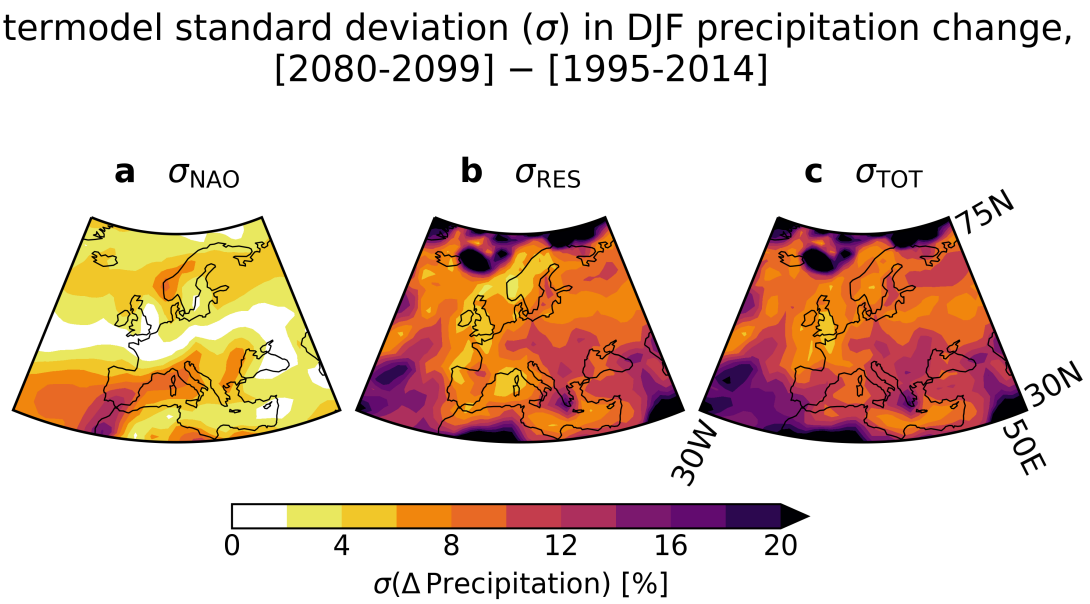

Figure S6: Maps of the intermodel standard deviation, σ, in forced DJF precipitation projections (2080-2099 minus 1995-2014) for the MMLEA models. These maps are used to calculate Figure 1c. (a) The intermodel standard deviation in NAO-congruent forced precipitation change, σ_{NAO}, calculated from the "NAO" column in Figure S5. (b) The intermodel standard deviation in residual forced precipitation change, σ_{RES}, calculated from the "Residual" column in Figure S5. (c) The sum of panels (a) and (b), σ_{TOT}, where $\sigma_{TOT}^2 = \sigma_{NAO}^2 + \sigma_{RES}^2$; note this is very similar to the intermodel standard deviation in total forced precipitation change, calculated from the "Total" column in Figure S5. Figure 1c shows the fraction of total intermodel variance in forced precipitation projections that is NAO-congruent, calculated as $\sigma_{NAO}^2/\sigma_{TOT}^2$ from panels (a) and (c).

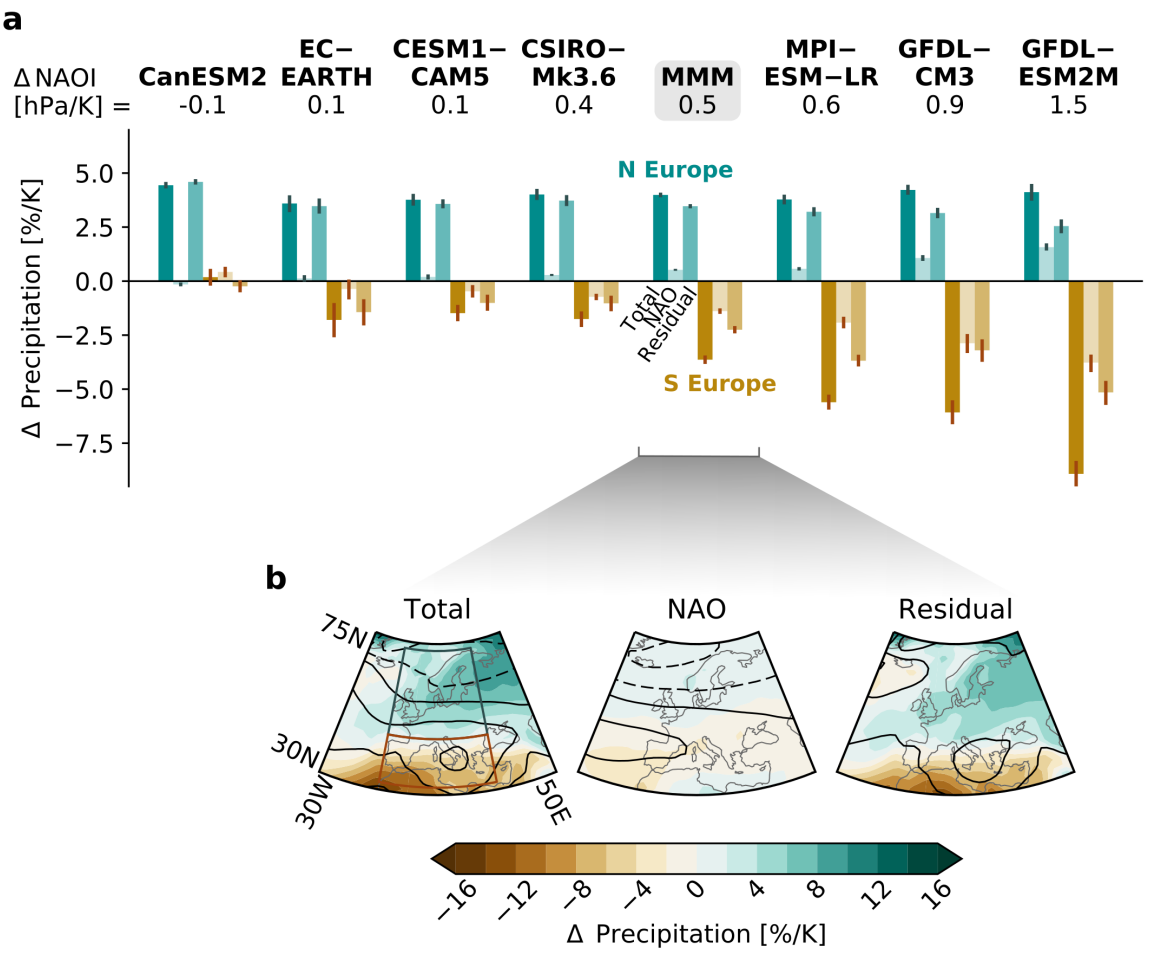

Figure S7: Same as Figure 1a-b, but where the precipitation and MSLP changes are normalized by the change in global-mean surface air temperature (GSAT). Models are ordered from left to right with increasing normalized forced DJF NAO index change (ΔNAOI); note this is a different order from Figure 1. GSAT changes from left to right are 4.3K (CanESM2), 3.6K (EC-EARTH), 4K (CESM1-CAM5), 3.8K (CSIRO-Mk3.6), 3.7K (MMM), 3K (MPI-ESM-LR), 4.5K (GFDL-CM3), and 2.5K (GFDL-ESM2M). Contours in (b) range from −0.6 hPa/K (dashed) to 0.6 hPa/K (solid) in 0.3 hPa/K intervals.

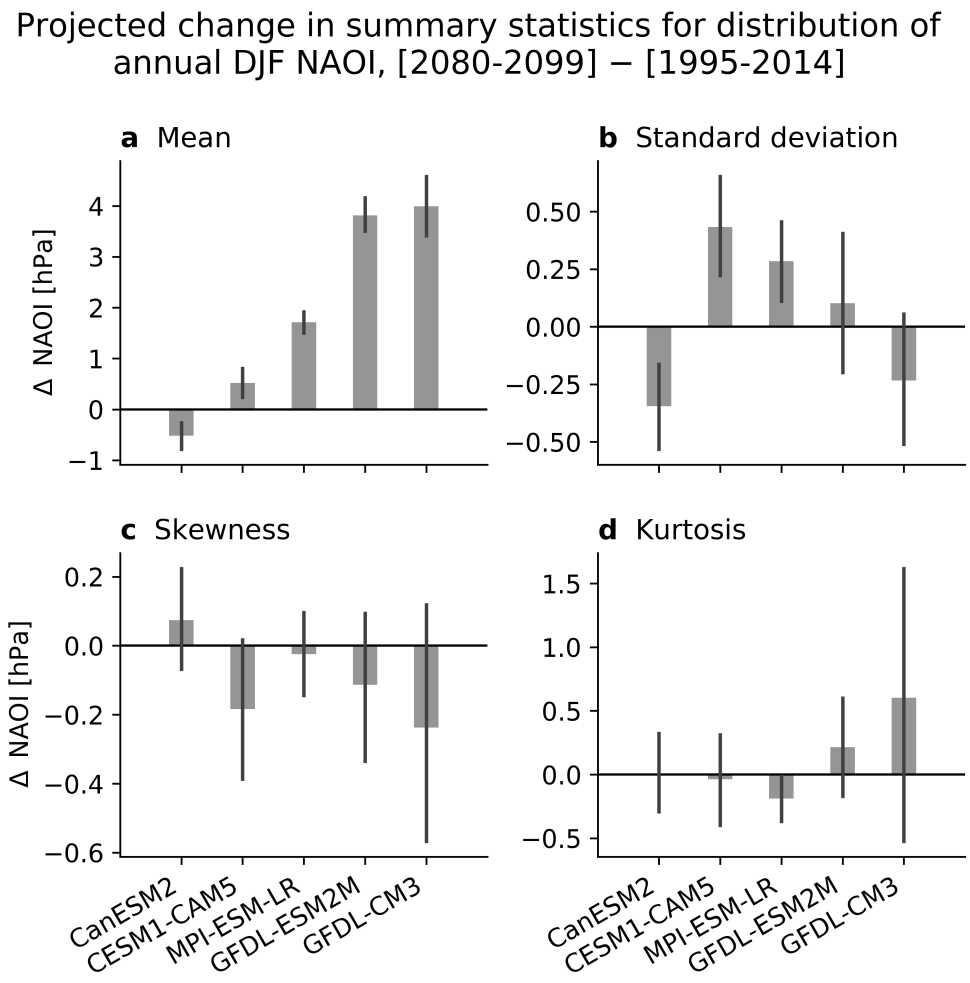

Figure S8: Projected change (2080-2099 minus 1995-2014) in the summary statistics for the distribution of annual DJF NAO index, for selected MMLEA models (see Section 3.1). The summary statistics evaluated are the (a) mean, (b) standard deviation, (c) skewness, and (d) kurtosis. Error bars show bootstrapped 95% confidence intervals.

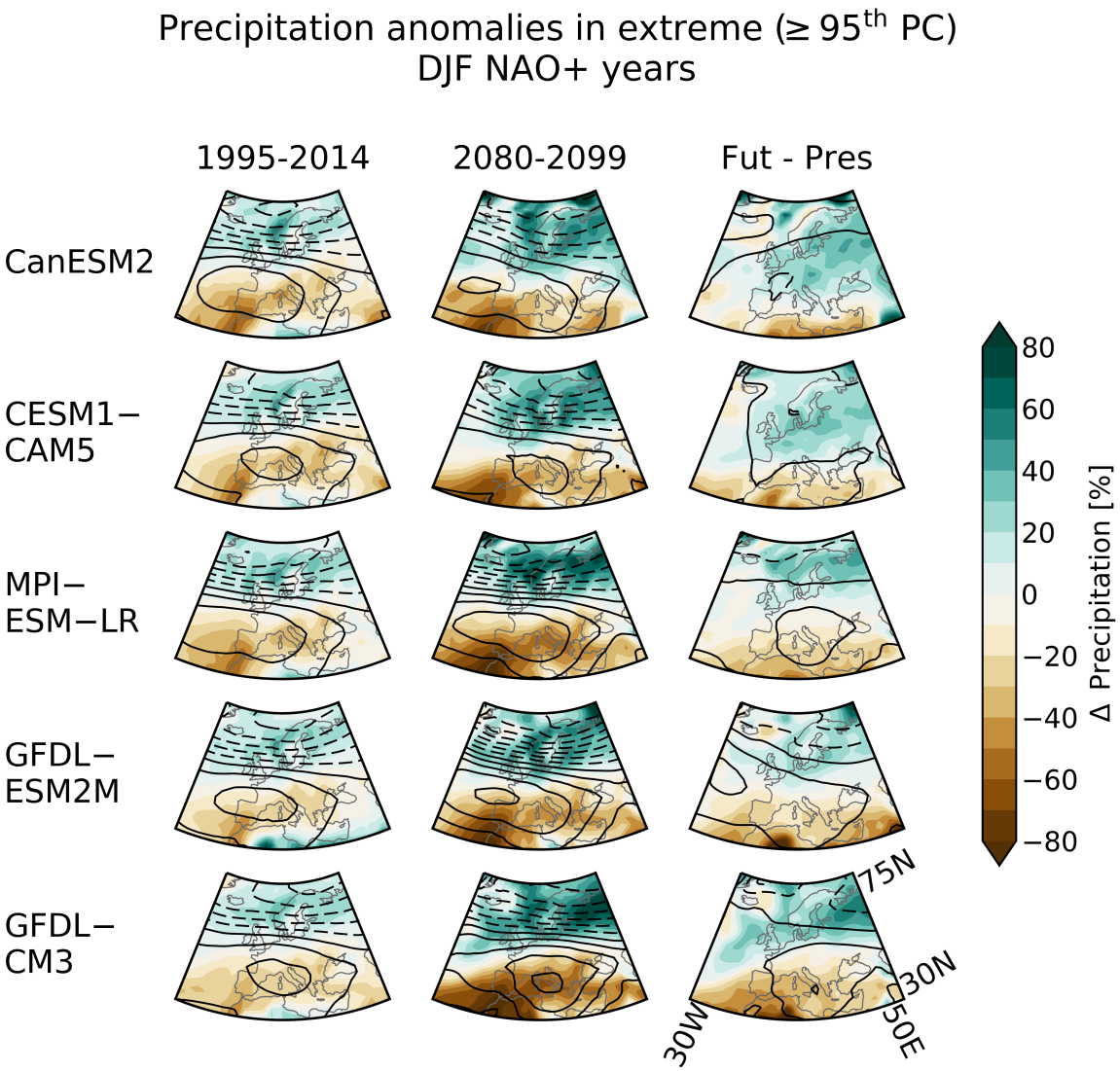

Figure S9: Maps in Figure 3b for all selected MMLEA models (see Section 3.1). Models are ordered from top to bottom with increasing mean DJF NAO index change. Contours range from −14 hPa (dashed) to 8 hPa (solid) in 2 hPa intervals.

Table S1. Details of the MMLEA model simulations used in the study. Simulations used are the historical and RCP8.5 runs. While the MMLEA does contain an ensemble for GFDL-ESM2M, for consistency with McKenna and Maycock (2021) we use a similar 30-member ensemble from the Princeton Large Ensemble Archive (Schlunegger et al., 2019).

Model	Modeling Center	Years	Number of members	Reference
CanESM2	CCCma	1950–2100	50	Kirchmeier-Young et al. (2017)
CESM1-CAM5	NCAR	1920–2100	40	Kay et al. (2015)
CSIRO-Mk3.6	CSIRO	1850–2100	30	Jeffrey et al. (2013)
EC-EARTH	EC-Earth Consortium	1860–2100	16	Hazeleger et al. (2010)
GFDL-CM3	GFDL	1920–2100	20	Sun et al. (2018)
GFDL-ESM2M	GFDL	1950–2100	30	Rodgers et al. (2015); Schlunegger et al. (2019)
MPI-ESM-LR	MPI	1850–2099	100	Maher et al. (2019)

Table S2. Details of the CMIP5 model simulations used in Figure S1. Simulations used are the historical and RCP8.5 runs. Numerical labels are for bars in Figure S1.

Label	Model	Modeling Center	Number of members	Members used
1	ACCESS1.0	CSIRO-BOM	1	r1i1p1
2	ACCESS1.3		1	r1i1p1
3	BCC-CSM1.1	BCC	1	r1i1p1
4	BCC-CSM1.1-M		1	r1i1p1
5	BNU-ESM	BNU	1	r1i1p1
6	CanESM2	CCCma	5	r1i1p1 – r5i1p1
7	CCSM4	NCAR	6	r1i1p1 – r6i1p1
8	CESM1-BGC	NSF-DOE-NCAR	1	r1i1p1
9	CESM1-CAM5		3	r1i1p1 – r3i1p1
10	CESM1-WACCM		3	r2i1p1 – r4i1p1
11	CMCC-CESM	CMCC	1	r1i1p1
12	CMCC-CM		1	r1i1p1
13	CMCC-CMS		1	r1i1p1
14	CNRM-CM5	CNRM-CERFACS	5	r1i1p1, r2i1p1, r4i1p1, r6i1p1, r10i1p1
15	CSIRO-Mk3.6.0	CSIRO-QCCCE	10	r1i1p1 – r10i1p1
16	EC-EARTH	ICHEC	7	r1i1p1, r2i1p1, r6i1p1, r8i1p1, r9i1p1, r12i1p1, r13i1p1
17	FGOALS-g2	LASG-CESS	1	r1i1p1
18	FIO-ESM	FIO	3	r1i1p1 – r3i1p1

Label	Model	Modeling Center	Number of members	Members used
19	GFDL-CM3	NOAA-GFDL	1	r1i1p1
20	GFDL-ESM2G		1	r1i1p1
21	GFDL-ESM2M		1	r1i1p1
22	GISS-E2-H	NASA-GISS	2	r1i1p1 – r2i1p1
23	GISS-E2-H-CC		1	r1i1p1
24	GISS-E2-R		2	r1i1p1 – r2i1p1
25	GISS-E2-R-CC		1	r1i1p1
26	HadGEM2-AO	NIMR-KMA	1	r1i1p1
27	HadGEM2-CC	MOHC	3	r1i1p1 – r3i1p1
28	HadGEM2-ES		4	r1i1p1 – r4i1p1
29	INM-CM4	INM	1	r1i1p1
30	IPSL-CM5A-LR	IPSL	4	r1i1p1 – r4i1p1
31	IPSL-CM5A-MR		1	r1i1p1
32	IPSL-CM5B-LR		1	r1i1p1
33	MIROC-ESM	MIROC	1	r1i1p1
34	MIROC-ESM-CHEM		1	r1i1p1
35	MIROC5		3	r1i1p1 – r3i1p1
36	MPI-ESM-LR	MPI-M	3	r1i1p1 – r3i1p1
37	MPI-ESM-MR		1	r1i1p1

Label	Model	Modeling Center	Number of members	Members used
38	MRI-CGCM3	MRI	1	r1i1p1
39	NorESM1-M	NCC	1	r1i1p1
40	NorESM1-ME		1	r1i1p1